High-power Yb-fiber comb based on pre-chirped-management self-similar amplification

Daping Luo, Yang Liu, Chenglin Gu, Chao Wang, Zhiwei Zhu, Wenchao Zhang, Zejiang Deng, Lian Zhou, Wenxue Li, and Heping Zeng

Citation: Appl. Phys. Lett. **112**, 061106 (2018); doi: 10.1063/1.5012100
View online: https://doi.org/10.1063/1.5012100
View Table of Contents: http://aip.scitation.org/toc/apl/112/6
Published by the American Institute of Physics

High-power Yb-fiber comb based on pre-chirped-management self-similar amplification

Daping Luo, Yang Liu, Chenglin Gu, Chao Wang, Zhiwei Zhu, Wenchao Zhang, Zejiang Deng, Lian Zhou, Wenxue Li,[a] and Heping Zeng[a]
State Key Laboratory of Precision Spectroscopy, East China Normal University, Shanghai 200062, China

(Received 6 November 2017; accepted 24 January 2018; published online 6 February 2018)

We report a fiber self-similar-amplification (SSA) comb system that delivers a 250-MHz, 109-W, 42-fs pulse train with a 10-dB spectral width of 85 nm at 1056 nm. A pair of grisms is employed to compensate the group velocity dispersion and third-order dispersion of pre-amplified pulses for facilitating a self-similar evolution and a self-phase modulation (SPM). Moreover, we analyze the stabilities and noise characteristics of both the locked carrier envelope phase and the repetition rate, verifying the stability of the generated high-power comb. The demonstration of the SSA comb at such high power proves the feasibility of the SPM-based low-noise ultrashort comb. *Published by AIP Publishing*. https://doi.org/10.1063/1.5012100

High-repetition optical frequency combs in the ultraviolet and mid-infrared regions can offer phase-stabilized low-noise optical sources for many scientific applications such as frequency metrology,[1–3] dual-comb spectroscopy,[4–6] efficient terahertz emission,[7] and astronomical calibration.[8] However, direct generation of high-repetition-rate pulses in ultraviolet and mid-infrared regions is a huge challenge due to the lack of suitable gain media. Fortunately, based on an available high-peak-power near-infrared comb, enhanced high harmonic generation (HHG),[9–11] optical parametric amplifier (OPA),[12] and difference frequency generation (DFG)[13,14] have potential to indirectly generate ultraviolet and mid-infrared combs. Especially, nonlinear applications based on high-power ultra-short combs, such as cavity-enhanced ultrafast spectroscopy[15] and four-wave-mixing spectroscopy,[16] have attracted much attention. Driven by these demands, the pulse amplification technique in the near-infrared region has been well developed in the past ten years. In particular, Yb-doped fibers have drawn much attention recently not only because of their good beam quality, high power-scaling capability, reliable compact structure, and excellent heat dissipation property but also because they can maintain the stabilities of the phase and the repetition rate during the amplification process. In 2008, an optical frequency comb with an average power of 10 W and a sub-millihertz linewidth was first demonstrated via a Yb-fiber amplification system.[17] Similarly, using a three-stage cascaded Yb-fiber chirped-pulse amplification system, they has also achieved an 80 W, 120 fs optical frequency comb.[18] Although these pulses are scaled up to dozens of watts through a chirped-pulse amplification system, the spectral width and pulse duration are limited by gain narrowing in amplification, restricting the applications of the pulses. Therefore, high-power fiber comb sources with a wider spectrum and a shorter pulse duration are desired.

In contrast to the chirped-pulse amplification, the proposed self-similar-amplification (SSA) can break the limitation of the gain bandwidth, leading to a shorter pulse duration and a wider spectrum. Mathematically, the pulse propagation in a fiber amplifier can be described by the gain-contained nonlinear Schrödinger equation (NLSE), yielding an asymptotic self-similar solution[19–21]

$$A(z,t) = A_p\left[1-\left(t/T_p\right)^2\right]^{1/2} e^{-iC_p t^2/2} e^{i\varphi_p(z)}, \quad |t| \le T_p,$$
$$A(z,t) = 0, \quad |t| > T_p, \tag{1}$$

$$A_p = (1/2)(gE_{in})^{1/3}(\gamma\beta_2/2)^{-1/6} e^{gz/3}, \tag{2}$$

$$T_p = 3g^{-2/3}E_{in}^{1/3}(\gamma\beta_2/2)^{1/3} e^{gz/3}, \tag{3}$$

$$C_p = g/(3\beta_2), \tag{4}$$

$$\varphi_p = \varphi_0 + 3\gamma(2g)^{-1}A_p^2, \tag{5}$$

where β_2 is the group velocity dispersion (GVD) parameter; γ is the nonlinear coefficient; g is the gain coefficient; E_{in} is the energy of the initial pulse; A_p, T_p, and φ_p are the amplitude, duration, and phase of the pulses at a position of z, respectively; and C_p is the linear chirp coefficient. Significantly, this solution reveals that linear-chirped parabolic pulses can propagate by a constant parabolic intensity profile with the introduction of linear chirp (C_p) and exponential power scaling (A^2_p) during the fiber amplification process. Moreover, due to an accumulated nonlinearity (little nonlinear phase shifting: φ_p–φ_0), a self-phase modulation (SPM) in the fiber will broaden the spectra beyond the gain bandwidth. For instance, a pulse train, with an average power of 100 W and a pulse duration of 60 fs, has been achieved utilizing a 90–μm large-pitch fiber.[22] Similarly, using a large-mode-area (LMA) Yb-doped photonics crystal fiber (PCF) SSA amplifier, the 80 W, 38 fs pulses with a high-quality beam have also been realized.[23] Moreover, with pre-chirp management of the group velocity dispersion (GVD) and third-order dispersion (TOD), we have demonstrated the generation of 93.5 W pulses with a pulse duration of 33 fs.[24] These SSA-based pulses exhibit good temporal and spectral characteristics, which are important for some scientific

[a]Authors to whom correspondence should be addressed: wxli@phy.ecnu.edu.cn and hpzeng@phy.ecnu.edu.cn

applications. Especially, it is proved that the phase property can be maintained in a self-similar amplifier with SPM.[25] Although the SSA of ultrashort pulses has been realized in many works, a high-power comb based on a SSA system has not been reported yet.

In this letter, we report on a fiber self-similar-amplification (SSA) comb system that delivers a 250 MHz 109 W 42 fs pulse train with a 10-dB spectra width of 85 nm at 1056 nm. A well-designed grism pair is employed to manage the GVD and TOD of pre-amplified pulses, leading to a self-similar evolution and a SPM. Significantly, this grism-based SSA system can realize near diffraction-limit pure pulses with a power of ~99.2% maintained in the main peak, which greatly facilitates phase stabilization.[26] After the locking of the carrier envelope phase (f_0) and repetition rate (f_r), a phase-stabilized optical frequency comb with an average power of more than one hundred watts is realized. Moreover, we discuss the frequency and noise characteristics of both f_0 and f_r, verifying the stability of this high-power comb.

Figure 1 shows the schematic of the experimental setup. A 250-MHz nonlinear-polarization-rotation mode-locked Yb-fiber oscillator was employed as the seed laser, which consisted of a 12-cm Yb-fiber (Yb406, CorActive), a 48-cm single-mode fiber (SMF, HI1060), and a 30-cm spatial part. By maintaining the cavity sum-dispersion around zero and a pump power of 600 mW, the oscillator operated in a low-noise regime,[27] outputting a 200-mW pulse train with a 68-nm-width spectrum centered at 1050 nm. In addition, the fiber in the cavity was mounted on a copper plate held at 23 °C by a thermoelectric cooler (TEC) module. To isolate the seed source from the environment, this whole resonant cavity was surrounded by a heat-insulation material together with a sound-insulation cotton and two layers of high-density aluminum plates. After transmission in a 50-m single-mode fiber (SMF, HI1060), the pulses were sufficiently stretched to dozens of picoseconds that could keep the next two pre-amplifiers operating under purely linear amplification, where the pulses were scaled up without introduction of nonlinear chirps. To meet the energy demands of SPM and self-similar evolution in the main amplifier, the pulses were scaled up in two preamplifiers, mainly consisting of a 20-cm single-mode Yb-fiber amplifier and a 1.5-m LMA Yb-doped PCF amplifier. The pre-amplifiers were pumped by two 976-nm semiconductor lasers with the pump powers of 0.6 and 25 W, respectively. After the two pre-amplifiers, these pulses were amplified to 12 W. In addition, an obvious spectral narrowing was observed due to the gain narrowing caused by the non-flat gain bandwidth of gain fibers.

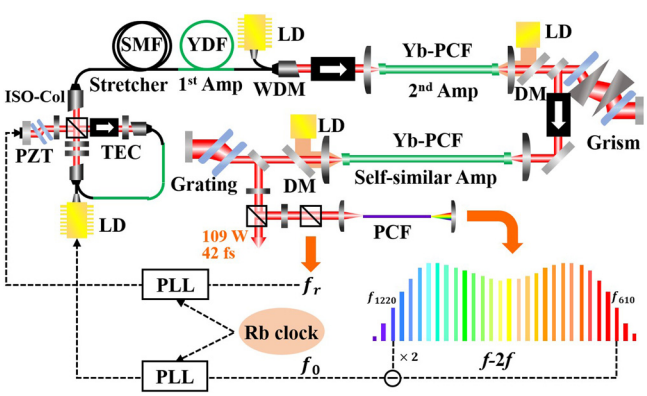

FIG. 1. Schematic of the experimental setup: PZT, piezo actuator; TEC, thermoelectric cooler; LD, diode laser; ISO-Col, collimator with an isolator; SMF, single-mode fiber; YDF, Yb-doped fiber; WDM, wavelength division multiplexer; Yb-PCF, Yb-doped photonic crystal fiber; DM, dichroic mirror; f_0, carrier envelope phase frequency; f_r, repetition rate frequency; and PLL, phase-locked loop.

Then, a pair of grisms, constructed with a pair of transmission gratings and a pair of equilateral prisms, was designed to compensate the GVD and TOD generated in the stretcher and pre-amplifiers. A fine dispersion management was carried out through adjusting the grating separation, prism insertion, and input angle. In particular, a dispersion material (ZF14), possessing an opposite TOD to the front fibers, was chosen to fabricate the prisms that facilitated the generation of diffraction-limit parabolic pulses. Then, 6 W reshaped pulses were delivered into a main amplifier with an efficiency of 90%, where power scaling, spectral widening, and temporal expansion were observed. This self-similar amplifier was composed of 2-m-long LMA Yb-PCF (NKT, DC-200–40-Yb), which was reversely pumped by a 200–μm-core pigtailed semiconductor laser (n-light, P2–200-975). On the pump end face, an approximate 235 W laser centered at 975 nm was coupled into the gain fiber. Moreover, the LMA PCF fibers with a core size of 40 μm were mounted on a copper plate held at 18 °C by a homothermal water-cooling setup. The cooling system guaranteed good power stability and relatively low intensity noise. To make up for the linear chirps produced in SSA, another pair of transmission gratings (800 lines/mm groove density) with high power handling was used to compress pulses with a total efficiency of more than 70%. Finally, high-power ultrashort pulses with a wide spectrum were realized via the coordination of the front grism pair and latter grating pair. In addition, all the end faces of the PM LMA Yb-PCFs were polished at a slant angle of 8° to minimize the back reflection, and three optical isolators were inserted among the seed laser and the amplifiers to avoid damage from the backward reflective light and the unabsorbed pumping light.

To characterize the properties of high-power SSA, the power curves of this amplifier and grating compressor are separately illustrated in Figs. 2(a) and 2(b). With a total of 235 W pump power coupled into a gain fiber, we achieve a pulse train of 154 W with an optical-to-optical efficiency of ~67%. These high power pulses are compressed by a pair of gratings with an output power more than 109 W and an efficiency of ~71%. As we can see, the efficiencies of both the SSA and the grating compressor exhibit good stability as the power increases. The spectral and temporal evolutions of pulses are shown in Figs. 2(c) and 2(d), respectively. The seed spectrum is centered at 1050 nm with a 10-dB bandwidth of 68 nm, corresponding to a pulse duration of 50 fs. After the grism pair, the spectrum is narrowed to 21 nm due to the gain narrowing effect in pre-amplifiers. Meanwhile, owing to the fine management of GVD and TOD, the pulses with a duration of 180 fs are obtained with ~99.9% power maintained in the main peak, greatly facilitating SSA and SPM in the main amplifier. As can be observed in Figs. 2(c) and 2(d), the SSA spectrum expands with the increasing output power because of SPM in the amplification process. Limited by an asymmetry gain profile of the gain fiber,

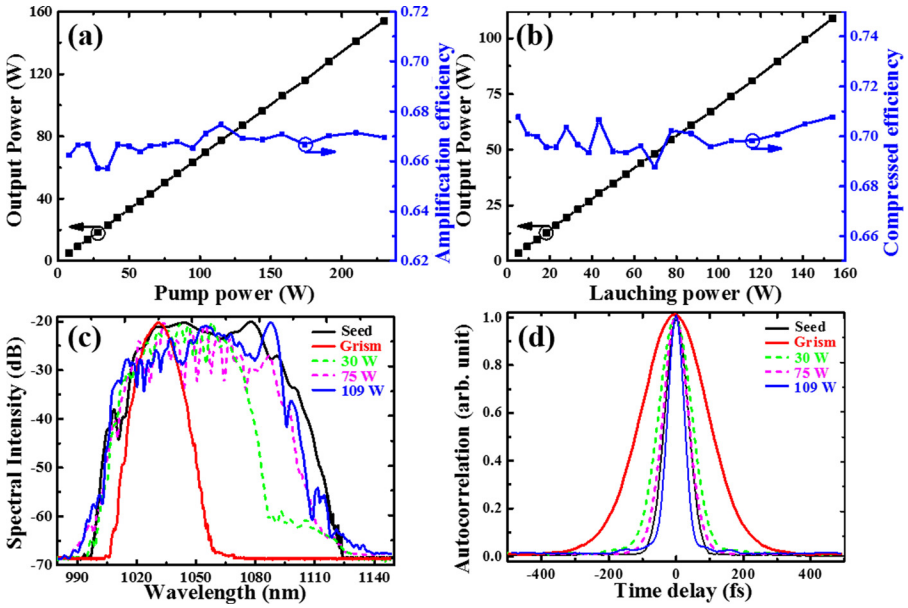

FIG. 2. (a) Output power (black line) and efficiency (blue line) of SSA versus pump power. (b) Output power (black line) and efficiency (blue line) of the grating compressor depending on the launching power. (c) and (d) Measured spectral (c) and temporal (d) properties after the seed (black line), grism (red line), and grating compressor with the powers of 30 W (green dash), 75 W (pink dash), and 109 W (blue line), respectively.

the output spectrum asymmetrically expands. Moreover, the spectral broadening in the main amplifier evolves with a smooth edge and a flat-top, showing a typical feature of self-phase evolution. When the output power increases to 109 W, the widest spectrum of 85 nm is achieved with a corresponding pulse duration of 42 fs. Furthermore, the compressed pulses are shorter than the initial pulses and have a similar pulse profile. These phenomena confirm the generation of linearly chirp and self-similar evolution. At the system-level max power, a few wings containing only an energy of ~0.8% of the pulse are observed on both sides of the main peak, which is crucial for the low-noise phase. Besides, no stimulated-Raman scattering is observed owing to the high repetition rate of 250 MHz, which supports a relatively low single-pulse energy.

Behind SSA, these pulses are divided into three parts by two polarization beam splitters (PBSs). A 50-mW part is delivered into a high-speed photoelectric detector for the detection of f_r. Another part of 500 mW is coupled into a 10-cm-long photonic crystal fiber for the generation of an octave-wide super-continuum spectrum. Then, a 610 nm component of ~200 μW and a 1220 nm component of 500 μW of the super-continuum spectrum are inputted to a self-reference f–$2f$ interferometer. After second harmonic generation (SHG) of 1220 nm, a ~50 μW second harmonic together with a ~50 μW component of the super-continuum spectrum at 610 nm is sent to a high-speed avalanche photodiode for the detection of f_0. As shown in Fig. 3(a), a beat signal of 20 MHz with a signal-to-noise ratio of more than 30 dB (100-kHz Video Band Width) is obtained through the f–$2f$ system. Then, the fourth-order harmonic frequency of the repetition rate ($4f_r$, 1 GHz) and the quartering frequency of the carrier envelope phase ($f_0/4$, 5 MHz) are chosen for two imported phase-locked loop circuits that can feedback control the pump current and PZT in cavity to lock the repetition rate and carrier envelope phase, respectively. After that, we separately lock $4f_r$ and $f_0/4$ to two standard radiofrequencies of 1 GHz and 5 MHz, both synchronized by a 10 MHz Rb clock. Moreover, we count the locked f_r and $f_0/2$ by a frequency counter, as depicted in Figs. 3(b) and 3(d). Over a total time of 1000 s, f_r and $f_0/2$ vary among 10 mHz and 6 mHz with the standard deviations of 1.32 mHz and 0.94 mHz, respectively, exhibiting good long-term stability. Figures 3(c) and 3(e) separately show the Allan deviations of f_r and $f_0/2$ as a function of average time. The fractional statistical uncertainties of f_r and $f_0/2$ for a 1000 s averaging time are 8.6×10^{-13} and 9.7×10^{-13}, which are mainly limited by the uncertainty of the Rb clock. These measurements confirm the generation of high-power combs, verifying the feasibility of the SPM-based SSA scheme.

To further investigate the stability of the high-power broadband comb, the noise curves of f_r and f_0 at powers of 30 W, 60 W, and 109 W are measured by a commercial phase noise analyzer. As shown in Fig. 4(a), intensity noises of f_0 are suppressed when the frequency is locked from a free-running state. However, the intensity noises increase slightly with a further increase in power, and the intensity noise curve at 109 W is even higher than the one in the 30-W unlocking situation. Figure 4(b) shows the phase noises of the locked f_0. The phase noises in a frequency region ranging from 1 Hz to ~3 kHz are strongly suppressed when f_0 is locked. Although the degeneration of phase noises is also observed as the power increases, the level of phase noises at the power of 109 W still characterizes good phase stability. Figures 4(c) and 4(d) show the noises of f_r. When we scaled up the average power, the intensity noises increased greatly, exactly as those of f_0. However, with the power scaling, the phase noises hardly increased. The reason was that f_0 was more sensitive to the disturbances from the amplification process than f_r due to different detection setups. Therefore, the same disturbance could add more phase noises in f_0 than in f_r. These degenerations of noises are mainly rooted in the fiber temperature variation, power shaking, and pump wavelength shifting, which all increase with the rise in pump power. Fortunately, the level of these noises at a power of 109 W is also acceptable for many scientific applications in the field of spectroscopy, providing an excellent high-power comb source.

Figure 5 shows the integrated noises of locked f_0 and f_r at the power of 109 W. After integration from 3 MHz to

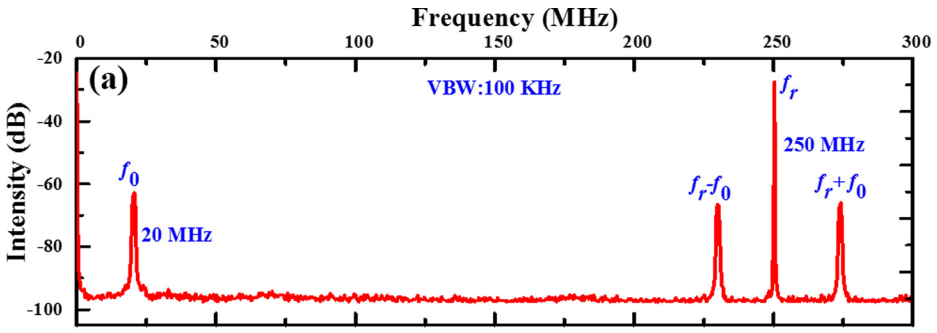

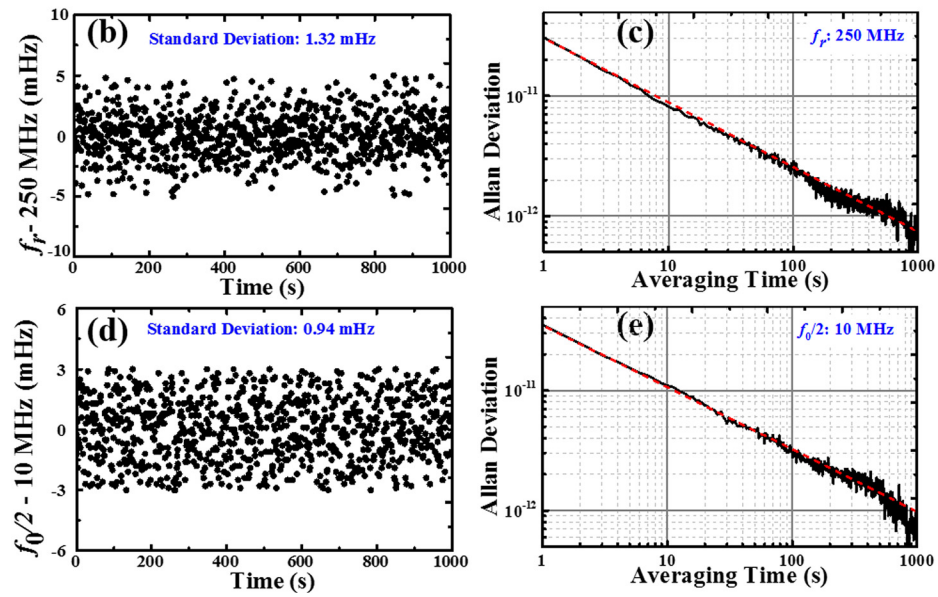

FIG. 3. (a) Radiofrequency spectrum of a self-reference *f*-2*f* interferometer related to the f_r and f_0 of 20 MHz and 250 MHz, respectively. Differences of f_r (b) and $f_0/2$ (d) versus measurement time and Allan deviation plots calculated from the time traces of f_r (c) and $f_0/2$ (e) are shown. A counter gate time of 1 s was used in the measurements.

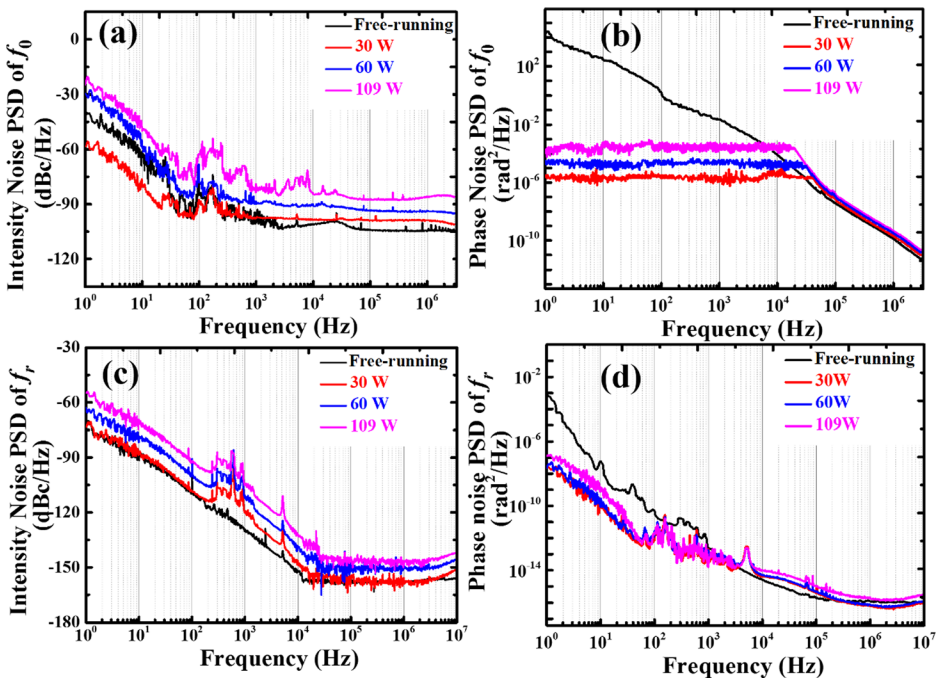

FIG. 4. Intensity (a) and phase noise (b) of a 20 MHz f_0 measured at a free-running condition with a power of 30 W (black line) and a phase-locked condition with powers of 30 W (red line), 60 W (blue line), and 109 W (pink line). (c) and (d) Intensity (c) and phase noises (d) of a 250 MHz f_r measured at a free-running condition with a power of 30 W (black line) and a phase stabilized condition with powers of 30 W (red line), 60 W (blue line) and 109 W (pink line).

1 Hz, the total intensity and phase noise of f_0 are 1.1% and 42 mrad, respectively. Similarly, the total intensity and phase noise of f_r are 0.05% and 8.5 mrad, respectively, with an integrated frequency ranging from 10 MHz to 1 Hz. These noise curves of f_0 and f_r characterize good stability of the high-power fiber comb. As far as we know, the noises of a comb at a power of more than one hundred watts have never been reported. Therefore, these noise curves measured at a power of 109 W, described in Figs. 4 and 5, can provide a visual reference for the relevant noise analysis of a high-power comb.

In summary, we demonstrate a generation of a SSA comb system, outputting a 42 fs, 85 nm phase-stabilized pulse train with a center wavelength of 1056 nm and a

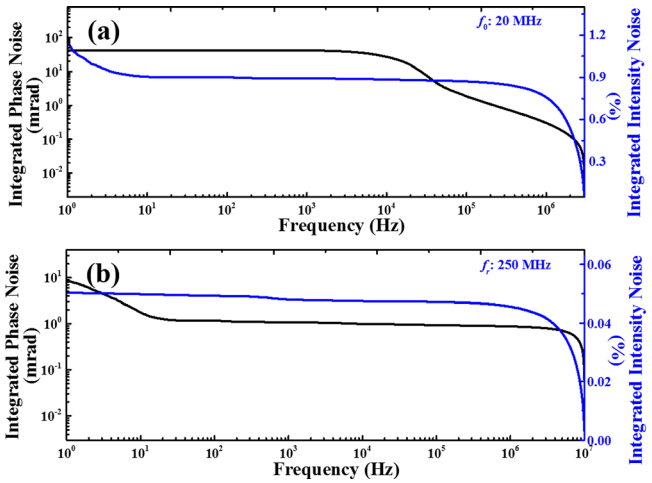

FIG. 5. (a) Integrated phase (black line) and intensity (blue line) noises of f_0 at a power of 109 W. (b) Integrated phase (black line) and intensity (blue line) noises of f_r at a power of 109 W.

repetition rate of 250 MHz. In detail, a pair of grisms is used to compensate the GVD and TOD generated in pre-amplifiers for the generation of near-parabolic pulses, which will lead to self-similar evolution and SPM in the main amplifier. Behind the SSA system, pure pulses with a power of ~99.2% maintained in the main peak were obtained. After the detection and locking of f_0 and f_r, a phase-stabilized optical frequency comb with an average power of 109 W is realized. To verify the stability of this high-power comb, we analyze the frequency stability and noise characteristics of both locked f_0 and f_r, revealing that the SPM and SSA comb can exhibit an low noise and frequency stability at the power level more than one hundred watts. This kind of comb would be employed as an optical source for the generation of ultraviolet and mid-infrared combs in the future and also could be applied in astronomical metrology, bio-imaging, and molecular spectroscopy.

This work was partly supported by the National Natural Science Foundation of China (11422434 and 11621404); the National Key Scientific Instrument Project (2012YQ150092), Shanghai Municipal Education Commission, and Shanghai Education Development Foundation (16SG22).

[1]T. Udem, R. Holzwarth, and T. W. Hänsch, Nature **416**, 233–237 (2002).
[2]A. Cingöz, D. C. Yost, T. K. Allison, A. Ruehl, M. E. Fermann, I. Hartl, and J. Ye, Nature **482**, 68–71 (2012).
[3]M. Vainio and J. Karhu, Opt. Express **25**, 4190–4200 (2017).
[4]B. Bernhardt, A. Ozawa, P. Jacquet, M. Jacquey, Y. I. Kobayashi, T. Udem, R. Holzwarth, G. Guelachvili, T. W. Hänsch, and N. Picqué, Nat. Photonics **4**, 55–57 (2010).
[5]Z. Zhang, T. Gardiner, and D. T. Reid, Opt. Lett. **38**, 3148–3150 (2013).
[6]I. Coddington, N. Newbury, and W. Swann, Optica **3**, 414–426 (2016).
[7]W. M. Wang, S. Kawata, Z. M. Sheng, Y. T. Li, L. M. Chen, L. M. Qian, and J. Zhang, Opt. Lett. **36**, 2608–2611 (2011).
[8]T. Steinmetz, T. Wilken, C. Araujo-Hauck, R. Holzwarth, T. W. Hänsch, L. Pasquini, A. Manescau, S. D'Odorico, M. T. Murphy, T. Kentischer *et al.*, Science **321**, 1335–1337 (2008).
[9]H. Carstens, M. Högner, T. Saule, S. Holzberger, N. Lilienfein, A. Guggenmos, C. Jocher, T. Eidam, D. Esser, V. Tosa, V. Pervak *et al.*, Optica **3**, 366–369 (2016).
[10]A. K. Mills, S. Zhdanovich, A. Sheyerman, G. Levy, A. Damascelli, and D. J. Jones, Proc. SPIE **9512**, 95121I (2015).
[11]T.-H. Wu, D. R. Carlson, and R. J. Jones, Frontiers in Optics 2013, Orlando, FL, 6–10 October 2013, paper FTu2A.4.
[12]C. Zhang, P. Wei, Y. Huang, Y. Leng, Y. Zheng, Z. Zeng, R. Li, and Z. Xu, Opt. Lett. **34**, 2370–2372 (2009).
[13]G. Soboń, T. Martynkien, P. Mergo, L. Rutkowski, and A. Foltynowicz, Opt. Lett. **42**, 1748–1751 (2017).
[14]A. Ruehl, A. Gambetta, I. Hartl, M. E. Fermann, K. S. E. Eikema, and M. Marangoni, Opt. Lett. **37**, 2232–2234 (2012).
[15]B. Lomsadze and S. T. Cundiff, Opt. Lett. **42**, 2346–2349 (2017).
[16]M. A. R. Reber, Y. Chen, and T. K. Allison, Optica **3**, 311–317 (2016).
[17]T. R. Schibli, I. Hartl, D. C. Yost, M. J. Martin, A. Marcinkevic, M. E. Fermann, and J. YE, Nat. Photonics **2**, 355–359 (2008).
[18]A. Ruehl, A. Marcinkevicius, M. E. Fermann, and I. Hartl, Opt. Lett. **35**, 3015–3017 (2010).
[19]M. E. Fermann, V. I. Kruglov, B. C. Thomsen, J. M. Dudley, and J. D. Harvey, Phys. Rev. Lett. **84**, 6010–6013 (2000).
[20]C. Finot, F. Parmigiani, P. Petropoulos, and D. J. Richardson, Opt. Express **14**, 3161–3170 (2006).
[21]S. Wang, B. Liu, C. Gu, Y. Song, C. Qian, M. Hu, L. Chai, and C. Wang, Opt. Lett. **38**, 296–298 (2013).
[22]W. Liu, D. N. Schimpf, T. Eidam, J. Limpert, A. Tünnermann, F. X. Kärtner, and G. Chang, Opt. Lett. **40**, 151–154 (2015).
[23]J. Zhao, W. Li, C. Wang, Y. Liu, and H. Zeng, Opt. Express **22**, 32214–32219 (2014).
[24]Y. Liu, W. Li, D. Luo, D. Bai, C. Wang, and H. Zeng, Opt. Express **24**, 10939–10945 (2016).
[25]S. Wang, W. Chen, P. Qin, Y. Song, M. Hu, and B. Liu, Opt. Lett. **41**, 5286–5289 (2016).
[26]H. Liu, S. Cao, B. Lin, and Z. Fang, Opt. Commun. **381**, 403–408 (2016).
[27]L. Nugent-Glandorf, T. A. Johnson, Y. Kobayashi, and S. A. Diddams, Opt. Lett. **36**, 1578–1580 (2011).